Available online at www.sciencedirect.com
ScienceDirect
Computational Materials Science 41 (2008) 431–439
COMPUTATIONAL MATERIALS SCIENCE
www.elsevier.com/locate/commatsci

Extension of the temperature-related Cauchy–Born rule: Material stability analysis and thermo-mechanical coupling

Weixuan Yang [a], Shaoping Xiao [b,*]

[a] Department of Mechanical and Industrial Engineering, Center for Computer-Aided Design, The University of Iowa, 116 Engineering Research Facility, Iowa City, IA 52242, USA
[b] Department of Mechanical and Industrial Engineering, Center for Computer-Aided Design, The University of Iowa, 3131 Seamans Center, Iowa City, IA 52242, USA

Received 23 March 2007; received in revised form 26 April 2007; accepted 29 April 2007
Available online 29 June 2007

Abstract

In this paper, we first study the material stability of nanostructured materials via the continuum linearized stability analysis technique with the temperature-related Cauchy–Born (TCB) rule. As a temperature-related homogenization technique, the TCB rule considers the free energy instead of the potential so that temperature effects on material stability can be investigated. In addition, we develop a thermo-mechanical coupling model through implementing the thermal diffusion equation into nanoscale continuum approximation. Crack propagation at a nanoplate is studied as an example. Since the nanoscale phenomenon of bond breaking is involved when crack propagates, temperature increasing around the crack tip due to the released potential is considered in our thermo-mechanical coupling model.

PACS: 02.70.Ns; 46.15.−x; 61.82.Rx

Keywords: Homogenization; Temperature; Material stability; Thermo-mechanical coupling; Nanoscale continuum simulation; Fracture

1. Introduction

Although molecular dynamics [1–3] has been widely used to elucidate complex physical phenomena, it has limitations on both length and time scales. The recently developed multiscale methods [4–7] provide an alternative solution. Most multiscale methods at least contain a continuum model, in which the material properties are derived from the subscale, such as the nanoscale, via the homogenization technique. Consequently, the continuum approximation is used to approach a large group of atoms. However, most multiscale methods assume that there is zero temperature in the continuum model so that the stress is calculated from the nanoscale potential. Such an assumption results in difficultly studying temperature-related physical phenomena, including material failure, at the nanoscale via the continuum approximation. A temperature-related homogenization technique [8,9] proposed by Xiao and Yang provides one solution for the above issue. In addition, it is possible to conduct temperature-dependent material stability analysis and to develop a thermo-mechanical coupling model for nanoscale continuum approximation.

Material instability is always attractive to scientists and researchers in the domains of materials science and solid mechanics. Material instabilities usually occur in nonassociative plasticity and softening materials where stress decreases with increasing strain. In the early work of Hadamard [10], he identified the conditions for a vanishing propagation speed of an acceleration wave as a material instability when the tangent modulus is negative. Hill [11] considered an infinite body of the material in a homogeneous state of stress and deformation and then applied a

* Corresponding author. Tel.: +1 319 3356009; fax: +1 319 3355669.
E-mail address: shaoping-xiao@uiowa.edu (S. Xiao).

0927-0256/$ - see front matter © 2007 Elsevier B.V. All rights reserved.
doi:10.1016/j.commatsci.2007.04.023

small perturbation to the body and obtained an expression for its response. He concluded that if the perturbation grew, the material was considered unstable; otherwise, it was stable. Ogden [12] further showed that material instability in equilibrium problems was associated with loss of ellipticity of the incremental equations of equilibrium. In general, loss of ellipticity will always occur when the tangent modulus loses positive-definiteness, although it is possible to lose the ellipticity condition when the tangent modulus is positive-defined.

Elliott and co-workers [13,14] have discussed the stability theories of crystalline solids using multilattice kinematics. They classified three different stability criteria: the phonon stability, the homogenized continuum (HC) stability, and the Cauchy–Born (CB) stability. The phonon stability is defined in terms of the normal modes of atomic vibration (phonons) in a crystal solid. It considers the largest set of perturbations and indicates stability with respect to bounded perturbations of all wavelengths at the atomic scale. Therefore, the phonon stability is based on the nanoscale point of view. As a difference from the phonon stability, both the HC stability and the CB stability consider material stability when the crystal solid is subject to a continuum-level deformation gradient. If a crystalline solid containing a complex lattice, such as a Bravais multilattice, is subject to a deformation gradient, its deformed configuration cannot be represented by one basic nucleus and two simple Bravais lattice vectors. Therefore, a shift vector, called the inner displacement, must be introduced. The role of the inner displacement in analyzing material stability determines whether using the HC stability or the CB stability.

If the inner displacement has insignificant effect on material stability, the HC stability should be employed. Indeed, the HC stability criterion indicates stability with respect to all internally equilibrated "uniform" perturbations at the macroscopic continuum scale. A "homogenized continuum" energy density is defined as a function only of the deformation gradient by eliminating the inner displacements using energy minimization. The CB stability provides an intermediate criterion by considering perturbations at both the atomistic and continuum scales. It indicates stability with respect to all "quasi-uniform" perturbations and includes HC stability as a special case. In the CB stability, both the uniform deformation gradient and the inner displacements are allowed to vary independently. In this paper, we mainly consider the HC stability. According to the HC stability, the crystal's equilibrium configuration is considered stable if the resulting elastic moduli are positive definite with respect to all deformation gradients. The HC stability criterion is identical to the strong ellipticity condition and hyperbolicity condition for the time-dependent PDE.

In numerical modeling and simulation, the temperature-related homogenization technique can help to evaluate stress at a local material point if the temperature profile is prescribed. However, material failure is always related to bond breaking at the nanoscale, in which the released energy results in temperature increase in the surrounding material during formation and propagation of cracks. Therefore, a thermo-mechanical model must be developed via coupling the energy equation with the momentum equations in the nanoscale continuum approximation. In this paper, we couple the thermal diffusion equation in the nanoscale meshfree particle method [9,15]. The temperature profile is updated via solving discrete equations of thermal flow. Since locally thermal dynamic equilibrium is assumed, the TCB rule is still valid for calculating stresses for solving equations of motion. If crack nucleates and propagates, the released energy due to bond breaking at the nanoscale will be used to calculate the temperature increment in the continuum approximation.

This paper is outlined as follows. A new homogenization technique, the TCB rule, is described in Section 2. Temperature-related material stability analysis is performed in Section 3 to demonstrate temperature effects on material instability. In Section 4 a thermo-mechanical coupling model is introduced in the nanoscale meshfree particle method. Crack propagation in a nanoplate will be examined, followed by the conclusions.

2. Temperature-related Cauchy–Born rule

In order to investigate physical phenomena of the nanostructured materials via the continuum approach, homogenization techniques are expected to accurately extract the intrinsic mechanical properties of the material from the subscale, i.e., the nanoscale. The Cauchy–Born (CB) rule [16,17] is a widely used homogenization technique for modeling and simulating nanostructured materials. Using the CB rule, the strain energy density is computed from the potential at the nanoscale via the assumption of locally homogeneous deformation. Then, a constitutive relation can be derived and implemented into the continuum models in either hierarchical or concurrent multiscale methods. The main drawback of the CB rule is that it does not consider the temperature effects because the strain energy is calculated at 0 K. It has been shown that if the temperature effects on the mechanics of nanostructured materials are not significant, the continuum approaches are fairly good models compared with molecular mechanics simulations [6]. However, some molecular dynamics simulations indicated that temperature could reduce the strength of nanostructured materials [3] and introduce damping in nanodevices [2]. Therefore, a temperature-related homogenization technique is needed in physical-based nanoscale continuum approximations or multiscale modeling and simulations.

Xiao and Yang [8] have developed the temperature-related Cauchy–Born (TCB) rule, in which they considered the Helmholtz free energy instead of the strain energy so that the mechanics of nanostructured materials at finite temperatures could be investigated. Using the TCB rule, a temperature-dependent constitutive relation is derived as

$$\mathbf{P}(\mathbf{F},T)=\frac{\partial w_H(\mathbf{F},T)}{\partial \mathbf{F}}, \tag{1}$$

where w_H is the free energy density, and $\mathbf{P}$ is the continuum-level first Piola–Kirchhoff stress, which is a function of the deformation gradient, $\mathbf{F}$, and the temperature, T. Eq. (1) can serve as the stress–strain relation that can be implemented in most hierarchical and concurrent multiscale methods to investigate temperature-related physical behaviors of nanostructured materials.

In the TCB rule, besides the assumption of locally homogeneous deformation, which is the same as in the conventional CB rule, there are other assumptions, as follows: (1) atoms have the same local vibration modes, (2) the vibration of an atom is harmonic, and (3) coupled vibration of different atoms is negligible. Generally, if a nanostructured material contains N atoms at a temperature field of $T(\mathbf{X})$, the total free energy, W_H, when the material is subject to the gradient deformation $\mathbf{F}(\mathbf{X})$ can be calculated as

$$\begin{aligned} W_H(\mathbf{F},T) &= \int w_C(\mathbf{F})\mathrm{d}\Omega + n\kappa_{\mathrm{B}}\int \rho_n T\ln\left[\frac{\hbar(\overline{D}(\mathbf{F}))^{\frac{1}{2n}}}{\kappa_{\mathrm{B}}T}\right]\mathrm{d}\Omega \\ &= \sum_i^{N_q} w_C(\mathbf{F}_i^q)A_i + n\kappa_{\mathrm{B}}\sum_i^{N_q} n_i^q T_i^q \ln\left[\frac{\hbar(\overline{D}(\mathbf{F}_i^q))^{\frac{1}{2n}}}{\kappa_{\mathrm{B}}T_i^q}\right], \end{aligned} \tag{2}$$

where w_C is the strain energy density, i.e., the potential density at the nanoscale; n is the number of degrees of freedom per atom; κ_{B} is the Boltzmann constant; ρ_n is the number of atoms per unit volume; N_q is the number of quadrature points in the continuum model; A_i is the volume associated with one quadrature point, X_i^q, which represents n_i^q atoms; and $\hbar = h/2\pi$, where h is Planck's constant. $\overline{D}$ is the determinant of the local dynamic matrix:

$$D_{I\alpha J\beta}=\frac{1}{\sqrt{m_I m_J}}\left(\frac{\partial^2\varphi}{\partial x_{I\alpha}\partial x_{J\beta}}\right), \tag{3}$$

where $\varphi(\mathbf{x})$ is the potential energy of the atoms in their equilibrium positions, $x_{I\alpha}$ is the vibrational coordinate in direction α for atom I, and m_I is the mass of atom I. With the assumption in which atoms have local harmonic vibrations, the determinant of the local dynamic matrix can be calculated via diagonalization as

$$\overline{D}_I=\left(\prod_j^n \omega_{Ij}\right)^2, \tag{4}$$

where ω_j represents the principal frequencies of atom I and eigenvalues of the dynamic matrix.

It should be noted that the first term on the RHS of Eq. (2) was the continuum-level strain energy when temperature equaled zero. In the continuum model, the deformation gradient and the temperature are evaluated at each quadrature point. With the TCB technique, all the bonds and atoms in A_i are assumed to be at the same deformation and the same temperature. Consequently, the strain energy density, w_C, and the dynamic matrix can be calculated using the unit cell model for each quadrature point. The verification of the TCB rule has been conducted by Xiao and Yang [8,9].

3. Temperature-related stability analysis

With the implementation of the TCB rule, we study temperature effects on material stability using a linearized stability analysis technique [18]. This technique is equivalent to what is often called a von Neumann stability analysis, which is viewed as a standard stability analysis of the continuum. Note that only the momentum equation needs to be considered under a Lagrangian description, in which the material coordinates $\mathbf{X}$ are employed. To derive the linearized equation, we first assume that the perturbation of displacements is in the form of a plane wave

$$\tilde{\mathbf{u}}=\mathbf{g}\mathrm{e}^{\mathrm{i}\omega t+\mathrm{i}\kappa\mathbf{n}_0\cdot\mathbf{X}}, \tag{5}$$

where the superposed $\sim$ denotes the perturbation, $\mathbf{u}$ represents displacements, $\mathbf{g}$ is polarization of the wave, κ is wave number, ω is frequency, t is time, and $\mathbf{n}^0$ is the normal direction of the wave front with respect to the initial configuration. Consequently, the perturbation of deformation gradients is written as

$$\widetilde{F}_{kl}=\frac{\partial\tilde{u}_k}{\partial X_l}=\mathrm{i}\kappa g_k n_l^0\mathrm{e}^{\mathrm{i}\omega t+\mathrm{i}\kappa\mathbf{n}_0\cdot\mathbf{X}}. \tag{6}$$

Then, the perturbed governing equations are written as

$$\rho_0\ddot{\tilde{\mathbf{u}}}=\nabla_{\mathbf{X}}\cdot\widetilde{\mathbf{P}}^{\mathrm{T}}, \tag{7}$$

where ρ_0 is the initial density, the superposed dots denote material time derivatives, and $\nabla_{\mathbf{X}}$ is the gradient with respect to the material coordinate $\mathbf{X}$. $\widetilde{\mathbf{P}}$ is the perturbed first Piola–Kirchhoff stress tensor and it is calculated via the TCB rule:

$$\widetilde{\mathbf{P}}=\frac{\partial^2 w_H(\mathbf{F},T)}{\partial\mathbf{F}\partial\mathbf{F}}\cdot\widetilde{\mathbf{F}}=\mathbf{C}(\mathbf{F},T)\cdot\widetilde{\mathbf{F}}\quad\text{or}\quad\tilde{P}_{ij}=C_{ijkl}\tilde{F}_{kl}, \tag{8}$$

where $C_{ijkl}=\partial^2 w_H(\mathbf{F},T)/\partial F_{ij}\partial F_{kl}$ is the first tangential stiffness tensor and the second derivative of the free energy density with respect to the deformation gradient. Substituting Eqs. (5), (6) and (8) into Eq. (7) yields

$$-\rho_0\omega^2 g_i+\kappa^2 C_{jikl}n_j^0 n_l^0 g_k=0. \tag{9}$$

The condition for a nontrivial solution of the above equations is

$$\det\left[\omega^2\delta_{ik}-\frac{\kappa^2}{\rho_0}A_{ik}\right]=0, \tag{10}$$

where $A_{ik}=C_{jikl}n_j^0 n_l^0$ is the acoustic tensor. Eq. (10) is also taken as the characteristic equation for the continuum medium, and the stability of the material depends on the roots of this equation.

Generally, with a complex frequency, $\omega=\omega_R+\mathrm{i}\omega_I$, the perturbation of displacements can be rewritten as

$$\tilde{\mathbf{u}}=\mathbf{g}\mathrm{e}^{\mathrm{i}\omega t+\mathrm{i}\kappa\mathbf{n}_0\cdot\mathbf{X}}=\mathbf{g}\mathrm{e}^{-\omega_I t}\mathrm{e}^{\mathrm{i}(\omega_R t+\kappa\mathbf{n}_0\cdot\mathbf{X})}. \tag{11}$$

The above perturbed solution consists of two parts: one is the amplitude ($\mathbf{g}e^{-\omega_I t}$) and the other is a constant wave ($e^{i(\omega_R t+\kappa \mathbf{n}_0\cdot\mathbf{X})}$). Obviously, the imaginary part of the complex frequency, ω_I, governs the growth or decay of the perturbation. If ω_I is negative at any direction of propagation, i.e., $\forall \mathbf{n}^0$, the amplitude of the perturbation grows with time and the material becomes unstable. Otherwise, the material is stable.

Therefore, the material stability criterion can be written as

$$C_{jikl}n_j^0 n_l^0 h_i h_k > 0 \quad \forall \mathbf{h} \quad \text{and} \quad \mathbf{n}^0. \tag{12}$$

In other words, the positive-definiteness of the acoustic tensor for all $\mathbf{n}^0$ is sufficient for material stability (the imaginary part of the frequency ω vanishes, i.e., $\omega_I = 0$). Eq. (12) is the strong ellipticity condition, which is identical to the hyperbolicity condition for the time-dependent PDE and the HC stability criterion.

We first investigate the stability of a 1D molecule chain as an example. The Lennard-Jones 6–12 potential function is employed to describe the interatomic interaction between the nearest neighbored atoms:

$$\varphi(l) = 4\varepsilon\left[\frac{1}{4}\left(\frac{l_0}{l}\right)^{12} - \frac{1}{2}\left(\frac{l_0}{l}\right)^{6}\right], \tag{13}$$

where l is the deformed bond length, $l_0 = 1$ nm is the undeformed bond length, and $\varepsilon = 82.5$ aJ is the depth of the energy well. Each atom has a mass of 12 amu. Solving the characteristic equation in Eq. (10) or employing Eq. (12) results in the following stability criterion for the considered molecule chain:

$$\varphi''(F) + \frac{\kappa_B T}{2}\frac{\varphi^{(4)}(F)}{\varphi''(F)} - \frac{\kappa_B T}{2}\left[\frac{\varphi'''(F)}{\varphi''(F)}\right]^2 > 0. \tag{14}$$

The criterion of Eq. (14) is graphically demonstrated in Fig. 1 when the molecule chain is subject to tension. We consider various temperatures up to 3000 K. It can be seen that when the temperature increases, the stable domain gets smaller. For instance, if the molecular chain is subject to 9.5% strain, it becomes unstable when the temperature is larger than 750 K. We also conduct molecular dynamics simulations to verify the nanoscale continuum material stability analysis. A molecule chain containing 200 atoms is simulated. We simulate a number of cases at various tensile strains and temperatures. The Hoover thermostat [19] is used to maintain the molecule chain at the prescribed temperature. In each simulation, if the length of one bond is larger than the cutoff distance, 2.0 nm here, of the Lennard-Jones potential function, the molecule chain becomes unstable and broken. At this point, the potential of the molecule chain will be dramatically reduced. Otherwise, the molecule chain is at the thermodynamic equilibrium state, and it is stable. We use dots to represent stable cases for the molecule chain subject to a certain tensile strain at a given temperature in Fig. 1. We can see that the molecular dynamics results support the linearized stability analysis.

We next study the stability of 1-D molecular chains with different spring rates. The same Lennard-Jones potential function is employed as in Eq. (13). However, we vary the depth of the energy well so that molecular chains have different spring rates, i.e., stiffnesses. We consider three different depths of the energy well: 82.5 aJ, 41.25 aJ, and 8.25 aJ. It is evident that the potential function with a larger energy well depth results in a stiffer molecule chain. We first investigate stable domains of three molecule chains without considering temperature effects. In other words, the temperature is set as zero. In this case, the criterion of Eq. (14) is simplified as

$$\varphi''(F) > 0. \tag{15}$$

We find that those three molecule chains have the same stable domains, as shown in Fig. 2. To consider temperature effects, Eq. (14) is resolved to illustrate stable domains of three molecule chains in Fig. 2. It is evident that a stiffer molecule chain has a larger stable domain. We can also conclude that the temperature effect is less significant for a stiffer molecule chain.

We next consider a two-dimensional nanostructured material with a square lattice. The Lennard-Jones potential

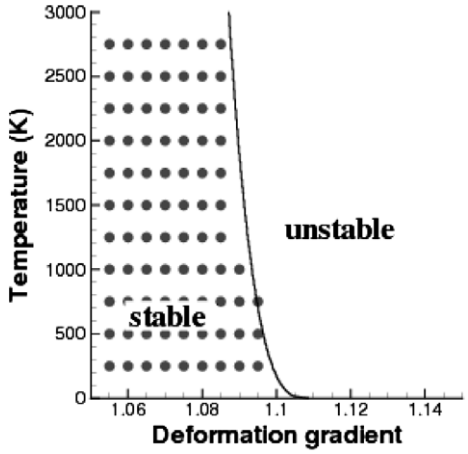

Fig. 1. Stable domain of 1-D molecule chain.

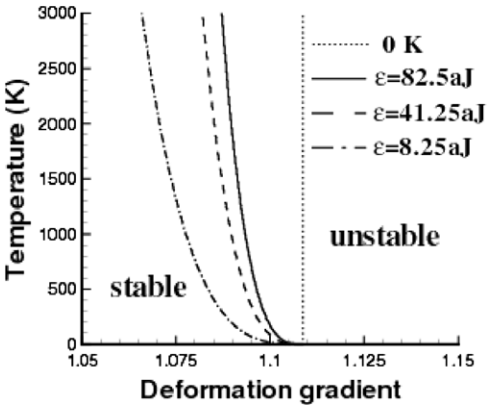

Fig. 2. Stability of 1-D molecule chains with different spring rates.

in Eq. (13) is still used here to describe bonded interatomic interactions. Using the TCB rule, the first tangential stiffness tensor is calculated as

$$\mathbf{C} = \frac{\partial^2 w_C}{\partial \mathbf{F} \partial \mathbf{F}} + \frac{1}{A_0}\left(\frac{\kappa_B T}{2\overline{D}}\frac{\partial^2 \overline{D}}{\partial \mathbf{F}\partial \mathbf{F}} - \frac{\kappa_B T}{2\overline{D}^2}\frac{\partial \overline{D}}{\partial \mathbf{F}} \otimes \frac{\partial \overline{D}}{\partial \mathbf{F}}\right), \tag{16}$$

where w_C and $\overline{D}$ are the potential density and the determinant of the dynamical matrix calculated from a unit cell of the square lattice, respectively. A_0 is the area of this unit cell. In the criterion of Eq. (12), $n_1^0 = \cos\alpha$, $n_2^0 = \sin\alpha$, $h_1 = \cos\beta$, and $h_2 = \sin\beta$, where α and β are arbitrary angles. If Eq. (12) is invalid for any angle, the material is unstable. Here, we only consider the diagonal deformation gradient, $\mathbf{F} = \begin{bmatrix} \lambda_1 & 0 \\ 0 & \lambda_2 \end{bmatrix}$. The stable domains at various temperatures are shown in Fig. 3. We can see that the entire compressive domain ($0 < \lambda_i < 1$) is stable. However, for sufficiently large extensional deformations, the material is unstable. It is also evident that the stable domain is smaller at a higher temperature, the same conclusion as in the example of 1D molecule chains.

As a more practical example, we consider temperature effects on the material stability of a graphene sheet. A graphene sheet has a honeycomb multilattice, and the unit cell is shown in Fig. 4. It should be noted that the honeycomb multilattice is a Bravais multilattice, which has two types of basic nuclei shown as black and white dots in Fig. 4. Obviously, one basic nucleus and two simple Bravais lattice vectors cannot represent the entire lattice when the graphene sheet is subject to a homogeneous deformation. Therefore, the inner displacement, $\boldsymbol{\eta}$, as a shift vector must be introduced to define the relative displacement between the two types of basic nuclei. Consequently, the strain energy density is a function of inner displacements and deformation gradients. In this paper, we neglect the temperature effects on inner displacements since they are in the internal equilibrium. Similar to the work by Tadmor et al. [20], the inner displacement is calculated via the minimization of the strain energy density with respect to $\boldsymbol{\eta}$ for a given deformation of the lattice, i.e.,

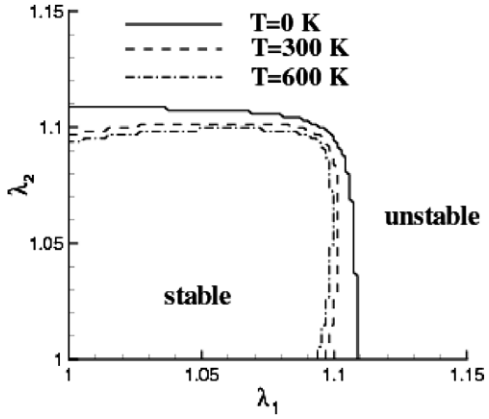

Fig. 3. Stable domains at various temperatures.

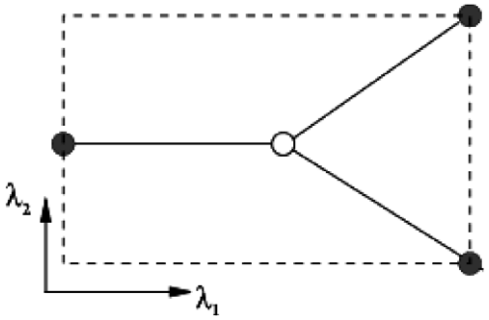

Fig. 4. The unit cell of a graphene sheet.

$$\boldsymbol{\eta}(\mathbf{F}) = \arg(\min_{\boldsymbol{\eta}} w_C(\mathbf{F}, \boldsymbol{\eta})) \Rightarrow \left.\frac{\partial w_C(\mathbf{F}, \boldsymbol{\eta})}{\partial \boldsymbol{\eta}}\right|_{\mathbf{F}} = 0. \tag{17}$$

In this example, we employ the modified Morse potential function [1] to describe the interatomic interaction. The first tangential stiffness tensor is calculated via the TCB rule as

$$\begin{aligned}\mathbf{C} &= \frac{\partial^2 w_H}{\partial \mathbf{F}\partial \mathbf{F}} + \frac{\partial^2 w_H}{\partial \mathbf{F}\partial \boldsymbol{\eta}}\frac{\partial \boldsymbol{\eta}}{\partial \mathbf{F}} = \frac{\partial^2 w_H}{\partial \mathbf{F}\partial \mathbf{F}} - \frac{\partial^2 w_H}{\partial \mathbf{F}\partial \boldsymbol{\eta}}\left(\frac{\partial^2 w_C}{\partial \boldsymbol{\eta}\partial \boldsymbol{\eta}}\right)^{-1}\frac{\partial^2 w_C}{\partial \boldsymbol{\eta}\partial \mathbf{F}} \\ &= \frac{\partial^2 w_C}{\partial \mathbf{F}\partial \mathbf{F}} + \frac{1}{A_0}\left(\frac{\kappa_B T}{2\overline{D}}\frac{\partial^2 \overline{D}}{\partial \mathbf{F}\partial \mathbf{F}} - \frac{\kappa_B T}{2\overline{D}^2}\frac{\partial \overline{D}}{\partial \mathbf{F}} \otimes \frac{\partial \overline{D}}{\partial \mathbf{F}}\right) \\ &\quad - \left[\frac{\partial^2 w_C}{\partial \mathbf{F}\partial \boldsymbol{\eta}} + \frac{1}{A_0}\left(\frac{\kappa_B T}{2\overline{D}}\frac{\partial^2 \overline{D}}{\partial \mathbf{F}\partial \boldsymbol{\eta}} - \frac{\kappa_B T}{2\overline{D}^2}\frac{\partial \overline{D}}{\partial \mathbf{F}} \otimes \frac{\partial \overline{D}}{\partial \boldsymbol{\eta}}\right)\right]\left(\frac{\partial^2 w_C}{\partial \boldsymbol{\eta}\partial \boldsymbol{\eta}}\right)^{-1} \\ &\quad \times \frac{\partial^2 w_C}{\partial \boldsymbol{\eta}\partial \mathbf{F}},\end{aligned} \tag{18}$$

where A_0 is the area of the unit cell. Then, the stability of a graphene sheet can be determined via Eq. (12). During our analyses, we find that if the graphene sheet is subject to deformation on the direction of λ_1, shown in Fig. 4, the inner displacement plays a significant role in the stability of the graphene sheet. In this case, the CB criterion [13,14] has to be applied. In this paper, we only conduct stability analysis when the graphene sheet is subject to elongation on the direction of λ_2, i.e., $\lambda_1 = 1$, because the effect of the inner displacement can be neglected. It should be noted that the λ_2 direction coincides to the axial direction of an armchair carbon nanotube. Since size effects of large armchair carbon nanotubes can be negligible [21], stability analysis performed here can assist in the prediction of failure strains of armchair nanotubes, as shown in Fig. 5. It can be seen that at the room temperature of 300 K, the failure strain is 13.5%. Taking the average secant Young's modulus [21] of 800 GPa for carbon nanotubes, the failure stress of armchair tubes at room temperature is 108 GPa, which is in good agreement with molecular dynamics simulation, 110 GPa [3].

4. Thermo-mechanical coupling model

To develop a thermo-mechanical coupling model in nanoscale continuum simulations, the energy equation

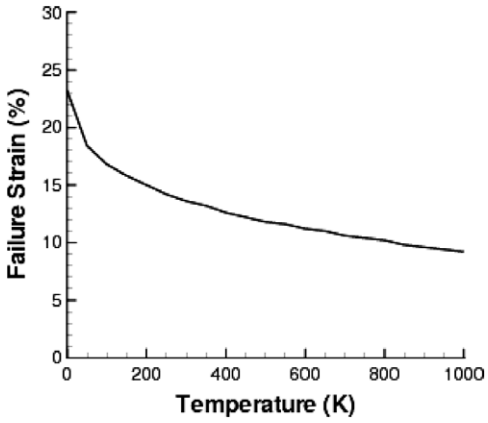

Fig. 5. Predicted failure strains of armchair carbon nanotubes.

should be considered as well as the temperature-related homogenization techniques. When assuming Fourier's law for heat conduction, the energy equation is

$$\rho\bar{c}\dot{T} = \sigma_{ij}v_{i,j} + k\nabla^2 T + S, \tag{19}$$

where ρ is the density, $\bar{c}$ is the specific heat, T is the temperature, σ is the stress, v is the velocity, and k is the conductivity. If no internal heat source, S, exists and all deformations are reversible, the energy equation is rewritten as the macroscopic diffusion model for temperature profile.

In this paper, we mainly focus on nanoscale continuum simulation via the nanoscale meshfree particle method [9,15] to demonstrate the application of the proposed thermo-mechanical coupling model. In a two-dimensional problem subject to the Lagrangian description, the governing equations include the thermal diffusion equation and the momentum conservation equation

$$\rho_0 c_v \dot{T} = k\left(\frac{\partial^2 T}{\partial X^2} + \frac{\partial^2 T}{\partial Y^2}\right), \tag{20}$$

$$\rho_0 \ddot{u}_i = \frac{\partial P_{ji}}{\partial X_j} + \rho_0 b_i, \tag{21}$$

where ρ_0 is the initial density, c_v is the specific heat capacity, k is the thermal conductivity, $\mathbf{X}$ is the material (Lagrangian) coordinates, $\mathbf{u}$ is the displacement, $\mathbf{P}$ is the first Piola–Kirchhoff stress tensor, $\mathbf{b}$ is the body force per unit mass, and the superposed dots denote material time derivatives. The weak forms in the reference configurations, Ω_0, are written as follows via the Galerkin method:

$$\int_{\Omega_0} \delta T \rho_0 \dot{T} \mathrm{d}\Omega_0 = -\frac{k}{c_v}\int_{\Omega_0}\left(\frac{\partial(\delta T)}{\partial X}\frac{\partial T}{\partial X} + \frac{\partial(\delta T)}{\partial Y}\frac{\partial T}{\partial Y}\right)\mathrm{d}\Omega_0, \tag{22}$$

$$\int_{\Omega_0} \delta u_i \rho_0 \ddot{u}_i \mathrm{d}\Omega_0 = \int_{\Omega_0} \delta u_i \rho_0 b_i \mathrm{d}\Omega_0 - \int_{\Omega_0} \frac{\partial(\delta u_i)}{\partial X_j} P_{ij} \mathrm{d}\Omega_0 + \int_{\Gamma_0} \delta u_i \bar{t}_i \mathrm{d}\Gamma_0, \tag{23}$$

where δT and $\delta\mathbf{u}$ are the test functions, and $\bar{\mathbf{t}}$ is the prescribed boundary traction along the boundary, Γ_0. It should be noted that the boundary term in Eq. (22) vanished due to the essential boundary condition requirement.

We employ the nanoscale meshfree particle method in this paper to conduct nanoscale continuum simulations. In meshfree particle methods [22], the fields of temperature and displacements can be approximated as

$$T^h(\mathbf{X},t) = \sum_I w_I(\mathbf{X})T_I(t), \quad \mathbf{u}^h(\mathbf{X},t) = \sum_I w_I(\mathbf{X})\mathbf{u}_I(t), \tag{24}$$

where $w_I(\mathbf{X})$ are called Lagrangian kernels since they are functions of the material (Lagrangian) coordinates. The Lagrangian kernel functions can be obtained from the weight function, i.e.,

$$w_I(\mathbf{X}) = w(\mathbf{X}-\mathbf{X}_I) = \frac{W(\mathbf{X}-\mathbf{X}_I)}{\sum_K W(\mathbf{X}-\mathbf{X}_K)} \tag{25}$$

in which a quartic spline weight function is used:

$$W(R) = \begin{cases} 1 - 6\left(\frac{R}{R_0}\right)^2 + 8\left(\frac{R}{R_0}\right)^3 - 3\left(\frac{R}{R_0}\right)^4 & R \leqslant R_0, \\ 0 & R > R_0, \end{cases} \tag{26}$$

where $R = \|\mathbf{X}-\mathbf{X}_J\|$ and R_0 is the support radius of the influence domain.

Substituting Eq. (24) into the weak forms of Eqs. (22) and (23), the following discrete equations of thermal flow and motion can be obtained:

$$m_I \dot{T}_I = K_{IJ}T_J, \quad m_I = \rho_0 V_I^0, \tag{27}$$

$$m_I \ddot{u}_{iI} = f_{iI}^{\mathrm{ext}} - f_{iI}^{\mathrm{int}}, \tag{28}$$

where V_I^0 is the volume associated with particle I, K_{IJ} is the conductivity tensor as

$$K_{IJ} = -\frac{k}{c_v}\int_{\Omega_0}\left[\frac{\partial w_I(\mathbf{X})}{\partial X}\frac{\partial w_J(\mathbf{X})}{\partial X} + \frac{\partial w_I(\mathbf{X})}{\partial Y}\frac{\partial w_J(\mathbf{X})}{\partial Y}\right]\mathrm{d}\Omega_0, \tag{29}$$

and f_{iI}^{ext} and f_{iI}^{int} are the external and internal nodal forces, respectively, given by

$$f_{iI}^{\mathrm{ext}} = \int_{\Omega_0} \rho_0 w_I b_i \mathrm{d}\Omega_0 + \int_{\Gamma_0^t} w_I \bar{t}_i \mathrm{d}\Gamma_0, \tag{30}$$

$$f_{iI}^{\mathrm{int}} = \int_{\Omega_0} \frac{\partial w_I(X)}{\partial X_j} P_{ji} \mathrm{d}\Omega_0. \tag{31}$$

In the above integrals of Eqs. (29)–(31), we utilize the stress point integration scheme because the meshfree particle method with Lagrangian kernels and stress points is a stable numerical method [22,23]. It should be noted that temperatures might vary at different particles within thermal flow. However, a locally thermodynamic equilibrium is assumed so that the TCB rule is still valid to calculate stresses. Since the calculated first Piola–Kirchhoff stress is temperature-dependent, the internal forces computed in Eq. (31) are also temperature-dependent.

The flow chart of our simulation is as follows:

(a) Initialize the problem, including particle generation, boundary/initial condition definition, and material property identification.
(b) Solve the equations of thermal flow (Eq. (27)) and update particle temperatures.
(c) Calculate stresses at the positions of particles via the TCB rule, i.e., Eq. (1).
(d) Solve the equations of motion (Eq. (28)) and update particle displacements.
(e) Go to step (b) if the target time is not reached.
(f) Output.

In this paper, we restudy the problem of crack propagation in a nanoplate with triangular lattices [8], as shown in Fig. 6. As a difference from the one presented by Xiao and Yang [8], the temperature field is not prescribed. We give only an initial temperature, which is the room temperature of 300 K. Then, the temperature profile will be determined via solving Eq. (27) during the simulation. In this paper, the simulated nanoplate consists of 513,922 atoms with the following dimensions: the length of 1600 nm and the width of 280 nm. Each atom has the mass of 60 amu. An edge crack is initiated in the middle of the plate by taking out a number of bonds, and the initial crack length is 20 nm. The nanoplate is subject to fracture mode I via prescribed displacements with the strain rate of 1×10^{-8} per fs. In the meshfree particle model, there are 27,200 particles. The crack is modeled defining a line segment internal to the domain. The domains of influence for particles near the crack are truncated whenever they intersect the crack surface so that a particle on one side of the crack will not affect particles on the opposite side of the crack. This technique is called the visibility criterion by Krysl and Belytschko [24].

For simplification, the crack is restricted to propagate along the weak interface by assuming that only weakened bonds can be broken, as shown in Fig. 6. A Lennard-Jones

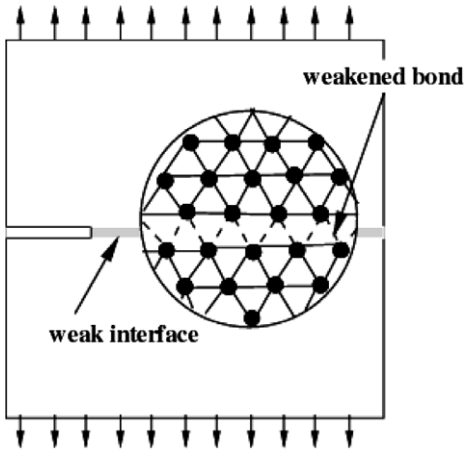

Fig. 6. A nanoplate with the triangular lattice containing an initial edge crack.

potential, i.e., $\varphi(l)$ in Eq. (13), with $\varepsilon = 2.47$ aJ, $l_0 = 1$ nm, and $l_{\text{cutoff}} = 2$ nm, is employed for weakened bonds. In the nanoplate except the weak interface, we use a harmonic potential function, $\varphi_{\text{h}}(l) = \frac{1}{2}k(l - l_0)^2$, to describe interatomic interactions between nearest neighboring atoms. The spring constant in this harmonic potential function is $k = 594.0$ nN/nm. Using the TCB rule, the first Piola–Kirchhoff stress, $\mathbf{P}$, at a particle, where the deformation gradient is $\mathbf{F}$ and the temperature is T, is calculated as follows based on a unit cell model [8,9]:

$$\mathbf{P} = \frac{\partial w_C}{\partial \mathbf{F}} + \frac{1}{A_0}\left(\frac{\kappa_{\text{B}} T}{2\overline{D}}\frac{\partial \overline{D}}{\partial \mathbf{F}}\right) = \frac{\partial w_C}{\partial \mathbf{F}} + \frac{\kappa_{\text{B}} T}{\sqrt{3}\overline{D} l_0^2}\frac{\partial \overline{D}}{\partial \mathbf{F}}. \tag{32}$$

It should be noted that both potential density, w_C, and the determinant of the dynamical matrix, $\overline{D}$, could be calculated via the unit cell model.

The thermal coefficients in equations of thermal flow, i.e., Eq. (27), are determined via molecular dynamics simulations on a piece of nanoplate. The specific heat capacity, c_v, represents how the system internal energy responds to an isometric change in temperature. We conduct two isometric molecular dynamics simulations with periodic boundary conditions on the testing nanoplate at various temperatures. In each simulation, the internal energy is computed as the time-averaged potential energy. Consequently, the specific heat capacity can be computed as the change of internal energy per unit temperature. The thermal conductivity k is the intensive property of a material that indicates its ability to conduct heat. It is defined as the quantity of heat, Q, transmitted in time t through a thickness L, in a direction normal to a surface of area A, due to a temperature difference ΔT, under steady state conditions and when the heat transfer is dependent only on the temperature gradient. In our simulation, we set a high temperature on one side of the testing nanoplate and a low temperature on the opposite side via the Hoover thermostat [19]. The periodic boundary condition is applied on the other two sides. The heat will transfer from the side with high temperature to the side with low temperature due to the temperature gradient. The total internal energy in the center part of the specimen is measured as a function of time, so that we can calculate the thermal conductivity via $k = QL/tA\Delta T$. For the simulated nanoplate, the following thermal coefficients are obtained: $c_v = 0.141$ J kg^{-1} K^{-1} and $k = 0.76$ W m^{-1} K^{-1}.

The crack propagation criterion used in our study is similar to the cohesive zone model [25]. Two crack tips are monitored in the cohesive zone model: one is physical tip, a "real" crack tip in physics, and the other is mathematical tip, a fictitious tip ahead of the physical one. The mathematical tip is used to determine the domain of influence in meshfree particle methods via the visibility criterion. Between the mathematical tip and the physical tip in the continuum model, there is a so-called cohesive zone, where the cohesive traction is applied on the two facets of the cohesive zone. The cohesive tractions, $\boldsymbol{\tau}$, are taken as

external forces in meshfree particle simulation and are derived via the TCB rule as

$$\boldsymbol{\tau} = \frac{\partial \hat{w}_H(\boldsymbol{\Delta}, T)}{\partial \boldsymbol{\Delta}} = \varphi'(\boldsymbol{\Delta}) + \frac{1}{2}\kappa_B T \frac{\varphi'''(\boldsymbol{\Delta})}{\varphi''(\boldsymbol{\Delta})}, \tag{33}$$

where φ is the Lennard-Jones potential describing the weak interface, $\boldsymbol{\Delta}$ is the crack opening displacement vector, and $\hat{w}_H(\boldsymbol{\Delta}, T)$ is the free energy per unit length along the cohesive zone. In meshfree particle methods, the cohesive tractions can be projected into consistent nodal forces [25] without introducing additional degrees of freedom.

At the nanoscale, crack initiation and propagation involve bond breakage. In this paper, we assume that the whole released potential due to bond breaking turns out to be the kinetic energy. We know that the kinetic energy at the nanoscale relates to the temperature, which is a macroscopic parameter. Consequently, the temperature increases due to the released energy. Since a bond is treated as broken when its deformed bond length exceeds the cutoff distance, the released energy is calculated as the difference between the potential when the bond length equals the cutoff distance l_{cutoff} and that when the bond length equals the equilibrium length l_0. In our simulation, the distance that the physical crack tip propagates determines the number of breaking bonds along the weak interface. Consequently, the temperature increment is thereafter calculated as follows:

$$\Delta T = \frac{1}{\kappa_B}\frac{\Delta\varphi_{\text{total}}}{N}, \tag{34}$$

where N is the number of atoms associated with the broken bonds and $\Delta\varphi_{\text{total}}$ is the total released energy. In nanoscale meshfree particle simulation, the increasing temperature is distributed on the particles around the physical crack tip based on the meshfree particle approximation. The temperatures on those particles will be treated as the discretized essential boundary conditions while solving the equations of thermal flow.

We simulate the crack propagation in the nanoplate subject to fracture mode I. The initial temperature is set as the room temperature of 300 K. The evolution of crack propagation speed is shown in Fig. 7. We can see that the crack starts to propagate at 0.42 ns. Once the crack propagates, some bonds along the weak interface are broken. The released energy results in a temperature increase in the surrounding domain around the crack tip. Furthermore, a temperature increase results in the reduction of cohesive traction in the cohesive zone along the weak interface. Consequently, the crack propagation speed increases gradually. Fig. 8 illustrates the temperature contour in the nanoplate at the time of 0.9 ns. The temperature concentration occurs around the crack tip, and temperature propagates from the crack tip to the remaining domain of the nanoplate. It should be noted that we designed a "fictitious" crystalline material with triangular lattices in this paper. This material can sustain high temperatures,

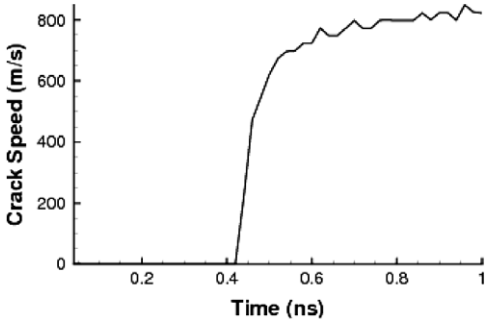

Fig. 7. Evolution of the crack propagation speed.

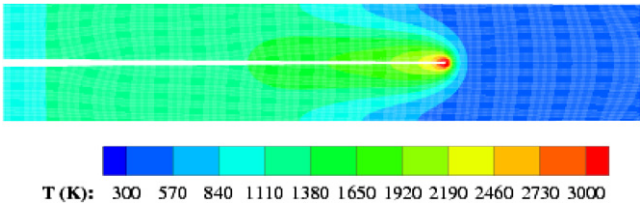

Fig. 8. Temperature contour at 0.9 ns.

such as 3000 K around the crack tip in Fig. 8, although 3000 K is higher than the melt temperatures of almost all existing single crystal materials.

5. Conclusions

We conducted stability analyses of nanostructured materials using a linearized stability analysis technique with a temperature-dependent homogenization technique, the TCB rule. In our material stability analyses, the continuum-level first tangential stiffness tensor was calculated from the free energy density instead of the potential density via the TCB rule so that the temperature effects were investigated. We concluded that nanostructured materials were more stable at lower temperatures and that at the same temperature stiffer materials could sustain larger deformation than softer materials. In particular, we predicted the failure strain of armchair carbon nanotubes at various temperatures via material stability analysis. The result at the room temperature of 300 K agreed with that calculated via molecular dynamics simulation. It should be noted that we used the linearized stability analysis technique, which is identical to the homogenized continuum stability criterion, in our paper because the inner displacement played an insignificant role in material instability. Otherwise, the Cauchy–Born stability criterion must be employed.

We also proposed a thermo-mechanical coupling model in which the thermal diffusion equation was discretized so that equations of thermal flow were solved to update the temperature profile during nanoscale continuum simulations. As an example, we employed the nanoscale meshfree particle method with the thermo-mechanical coupling model to study crack propagation in a nanoplate. Since bond breaking occurs at the nanoscale when crack propa-

gates, the total released energy resulting in the temperature increase around the crack tip was considered in our simulation. We found that crack speed increased gradually and high temperature concentration occurred around the crack tip. It should be noted that the thermal wave equation is a better physical model than the thermal diffusion equation to describe the temperature profile at the microscale. The similar strategy can be conducted to implement the thermal wave equation in the thermal–mechanical coupling model. In addition, there are other issues when implementing the thermo-mechanical coupling model in multiscale simulations because inter-scale heat transfer must be considered. Those issues will drive us to perform further research in this area.

Acknowledgement

The authors acknowledge support from the Army Research Office (Contract: # W911NF-06-C-0140).

References

[1] T. Belytschko, S.P. Xiao, G.C. Schatz, R. Ruoff, Phys. Rev. B 65 (2002) 235430.
[2] S.P. Xiao, D.R. Andersen, R. Han, W.Y. Hou, J. Comput. Theor. Nanosci. 3 (2006) 142–147.
[3] S. Xiao, W.Y. Hou, Phys. Rev. B 73 (2006) 115406.
[4] F. Abraham, J. Broughton, N. Bernstein, E. Kaxiras, Europhy. Lett. 44 (1998) 783–787.
[5] H.S. Park, E.G. Karpov, W.K. Liu, P.A. Klein, Philos. Mag. 85 (2005) 79–113.
[6] T. Belytschko, S.P. Xiao, Int. J. Multi. Comput. Eng. 1 (2003) 115–126.
[7] S.P. Xiao, T. Belytschko, Comput. Methods Appl. Mech. Eng. 193 (2004) 1645–1669.
[8] S.P. Xiao, W.X. Yang, Comput. Mater. Sci. 37 (2006) 374–379.
[9] S.P. Xiao, W.X. Yang, Int. J. Numer. Methods Eng. 69 (2007) 2099–2125.
[10] J. Hadamard, Leçons sur la propagation des ondes et les equations de l'hydrodynamique, Hermann, Paris, 1903 (Chapter 6).
[11] R. Hill, J. Mech. Phys. Solids 10 (1962) 1–16.
[12] R.W. Ogden, Non-linear Elastic Deformations, Dover, New York, 1997.
[13] R.S. Elliott, N. Triantafyllidis, J.A. Shaw, J. Mech. Phys. Solids 54 (2006) 161–192.
[14] R.S. Elliott, J.A. Shaw, N. Triantafyllidis, J. Mech. Phys. Solids 54 (2006) 193–232.
[15] S.P. Xiao, W.X. Yang, Int. J. Comput. Methods 2 (2005) 293–313.
[16] F. Milstein, Mechanics of Solids, in: H.G. Hopkins, M.J. Sewell (Eds.), Pergamon, Oxford, 1982.
[17] M. Arroyo, T. Belytschko, Mech. Mater. 25 (2003) 193–215.
[18] S.P. Xiao, T. Belytschko, Adv. Comput. Math. 23 (2005) 171–190.
[19] W.G. Hoover, Phys. Rev. A 31 (1985) 1695–1697.
[20] E.B. Tadmor, G. Smith, N. Bernstein, E. Kaxiras, Phys. Rev. B 59 (1999) 235–245.
[21] S.P. Xiao, W.Y. Hou, Fullerenes, Nanotubes Carbon Nanostruct. 14 (2006) 9–16.
[22] T. Rabczuk, T. Belytschko, S.P. Xiao, Comput. Methods Appl. Mech. Eng. 193 (2004) 1035–1063.
[23] T. Belytschko, S.P. Xiao, Comput. Math. Appl. 43 (2002) 329–350.
[24] P. Krysl, T. Belytschko, Int. J. Numer. Methods Eng. 44 (1999) 767–800.
[25] P.A. Klein, J.W. Foulk, E.P. Chen, S.A. Wimmer, H.J. Gao, Theor. Appl. Frac. Mech. 37 (2001) 99–166.